sustainability

MDPI

Article

Geometry and Kinematics of Northmost Yilan-Yitong Fault Zone, China: Insights from Shallow Seismic Data and Field Investigation

Qinghai Wei [1], Guanghao Ha [2,*], Wei Min [2] and Menghao Zhu [2,3]

[1] Heilongjiang Earthquake Agency, Harbin 150090, China
[2] Key Laboratory of Seismic and Volcanic Hazards, Institute of Geology, China Earthquake Administration, Beijing 100029, China
[3] China Geology Survey, Beijing 100037, China
* Correspondence: haguanghao@163.com or haguanghao@ies.ac.cn

Abstract: Detailed geological and geomorphological evidence has suggested that the Yilan-Yitong fault (YYF), one of the key branches of the Tancheng-Lujiang fault zone in northeastern China, has been an active fault since the Holocene that has extended from Liaoning Province to far-eastern Asia. However, there are no clear fault traces or late Quaternary active features northeast of Tangyuan County. In this study, we carried out shallow seismic reflection exploration, field geological investigation, and trench excavation across the YYF north of Tangyuan. The results revealed that the YYF is composed of two main branches: the west YYF branch is a late Pleistocene active fault, and the east one is a middle-to-early Pleistocene fault. In Heli Town, the west branch of YYF presents fault scarps with heights of ~0.6 m. Across the scarps, we excavated a trench, and we propose that the YYF displaced the late Pleistocene to Holocene deposits, as this was indicated by the geochronological data. The seismic reflection data and sedimentary sequence revealed that the YYF north of Tangyuan is composed of three tectonic belts: the western depression, the central bulge, and the eastern depression. Each tectonic belt is composed of several small folds formed from the end of the Paleogene to the beginning of the Neogene. After the Neogene, different subsidence and uplift events occurred in various parts of the YYF, and after the early Pleistocene, the fault showed a consistent subsidence.

Keywords: Yilan-Yitong fault; geometry and kinematics; seismic reflection profiles; late Quaternary active characteristics

check for updates

Citation: Wei, Q.; Ha, G.; Min, W.; Zhu, M. Geometry and Kinematics of Northmost Yilan-Yitong Fault Zone, China: Insights from Shallow Seismic Data and Field Investigation. *Sustainability* **2024**, *16*, 1943. https://doi.org/10.3390/su16051943

Academic Editors: Chong Xu, Su Chen and Shuang Li

Received: 11 September 2023
Revised: 23 December 2023
Accepted: 23 February 2024
Published: 27 February 2024

Copyright: © 2024 by the authors. Licensee MDPI, Basel, Switzerland. This article is an open access article distributed under the terms and conditions of the Creative Commons Attribution (CC BY) license (https://creativecommons.org/licenses/by/4.0/).

1. Introduction

The giant Tancheng-Lujiang fault zone (TLFZ), striking northeast, is located in the eastern margin of the Asian continent, which extends from southern China through the eastern part of the North China craton into the far east of Russia [1–5]. Due to its key location in a transition zone with a N–S compression tectonic regime between the Indian and Eurasian plates to the southwest and a nearly E–W extensional regime between the Pacific and Eurasian plates to the east, numerous geological, geophysical, and geochemical studies have been carried out focusing on the beginning, development, dynamic mechanism, metallogenic deposits, and earthquake disasters of this fault [6–18].

In northeast China, the Yilan-Yitong fault (YYF) and the Dunhua-Mishan fault (DMF) are considered to be the main branches of the TLFZ (Figure 1). More than 10 strong historical earthquakes have occurred along the TLFZ south of the Bohai Bay, whereas no $M \geq 6$ earthquakes have been recorded along the YYF or DMF. Moreover, the YYF was considered to be inactive since the late Quaternary due to the geographical conditions and artificial reconstruction until two paleoearthquake events were reported along the Fangzheng and Shulan segments of the YYF [10]. Then, research concerning the segmentation, paleoearthquakes, and late Quaternary slip rates of the YYF arose, which suggested that the YYF was an active dextral Holocene fault and could generate strong earthquakes ($M \geq 7$) [14]. South of Tangyuan County in Heilongjiang Province, the YYF is characterized

by an assemblage of landforms including linear scarps and troughs, offset or deflected streams, small horsts and grabens, and especially linear sag ponds [14]. North of the Tangyuan, however, the Luobei segment of the YYF has a large, unclear surface compared with the segment south of Tangyuan, which makes it difficult to define the location and late Quaternary active features of the Luobei segment.

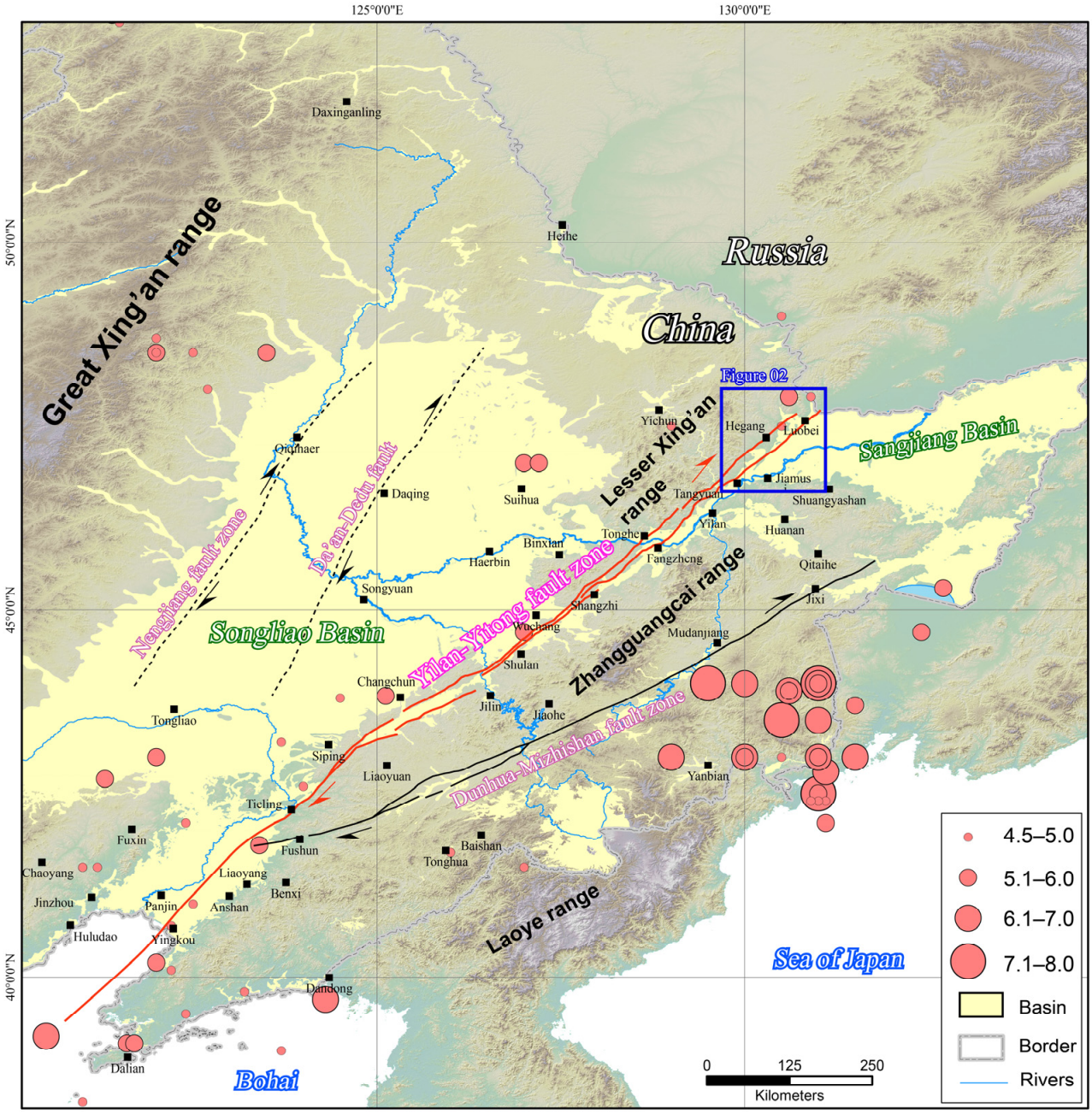

Figure 1. The extension and background of YYF and NE China. The blue rectangle shows the studied segment of YYF.

In this study, we conducted shallow seismic exploration and trench excavation across the YYF north of Tangyuan to map the geometry and kinematics of the fault.

2. Geological Background

As the largest fault in eastern China, the TLFZ controls the development and evolution of the crust and faults within the region, as well as the seismic activity [18,19]. According to the structures and active seismic features, the TLFZ can be divided into three segments: northern, central, and southern [19]. North of the Bohai Bay, the northern segment of TLFZ splits into the Yilan-Yitong fault to the north-northeast (NNE) and into the Dunhua-Mishan fault to the east-northeast (ENE). The southern-to-central TLFZ originated and experienced sinistral slip movement during the Triassic due to the collision between the North China craton and the South China block. Then, the TLFZ developed into NE China, forming the YYF in the early Cretaceous [19,20].

The NE-trending YYF runs from Shenyang, Changchun, and Harbin to far-eastern Asia and Russia. It is composed of two parallel branches with spacing of 10–30 km, resulting in a series of narrow grabens and uplifts (Figure 1) [20–22]. Four main grabens constitute the YYF; these are the Tangyuan, Fangzheng, Shulan, and Yilan grabens, bound by Songhuajiang, Shangzhi, and Yilan uplift from north to south, respectively [22]. The grabens are filled up with Paleogene to Neogene sandstone and mudstone overlaying lower-Cretaceous volcanics with angular unconformity [23–25]. During the Cenozoic, the YYF experienced a four-stage evolution progress: Paleogene rifting, compression-induced inversion at the end of the Paleogene, Neogene subsidence, and Quaternary compression. This was revealed by structural data and oil exploration results [22]. Although the proposed principal direction of compressive stress is still the subject of debate, the YYF was an oblique extensional graben in the Quaternary [7,22,26].

Geological and geomorphological evidence has revealed that the YYF has been active since the late Quaternary, presenting as a reverse and dextral strike–slip fault [9,14,15]. Trench excavation and geochronology identified that the latest paleoearthquake could have occurred in about AD 1810, with a magnitude of Ms 6.8–7.5 and seismic recurrence behavior, followed by a quasi-periodic pattern with a very long interval of 10–20 ka [14]. Geological and geomorphologic studies have suggested that the dextral slip rate of the YYF would have been ~0.2–0.3 mm/y, which is consistent with present geodetic observations [11].

At the northmost point, the YYF develops within the Tangyuan fault depression (TFD), which is a small petroleum basin west of the Sangjiang basin and northeast of China (Figure 2). The Cenozoic strata of TFD are occupied by Paleocene to Pliocene mudstone and sandstone and Quaternary sand and gravel [27]. A deep seismic reflection profile at the southern TFD demonstrated that the YYF was a lithospheric scale fault, with the Moho offset by the fault at a depth of 23–39 km [14]. Around TFD, the northern YYF is composed of two branches: the western YYF and eastern YYF, which separate the Zhangguangcai range massif to the northwest from the Jiamusi massif to the southeast (Figure 2).

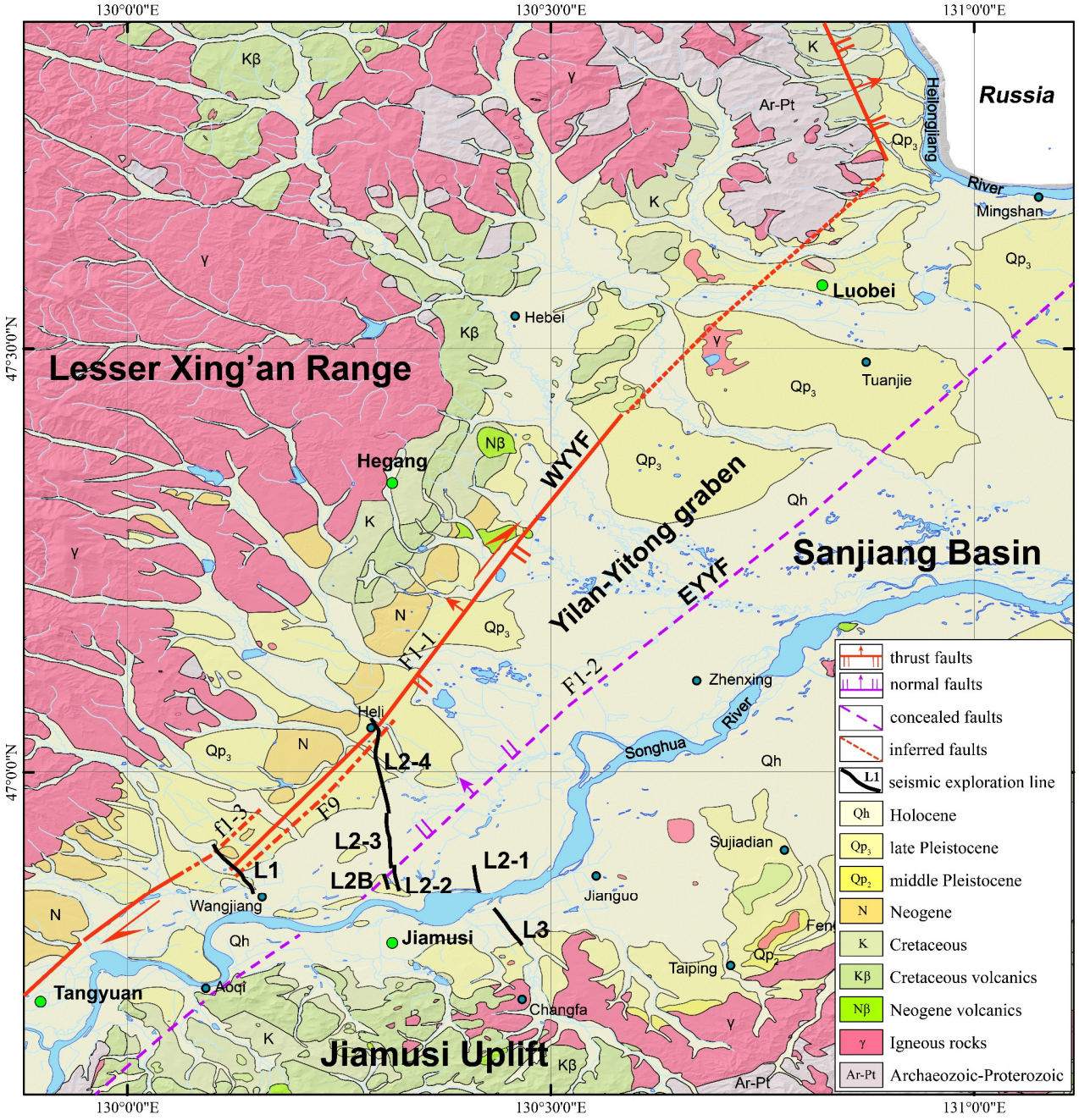

Figure 2. Geological map of YYF along the Tangyuan depression. WYYF: west Yilan-Yitong fault branch; EYYF: east Yilan-Yitong fault branch. The solid black lines show the seismic reflection profiles in this study.

3. Methods and Data

3.1. Seismic Reflection Data

To locate the northern YYF, we carried out 3 seismic reflection profile explorations across the fault zone using the longitudinal wave reflection method (Figure 2). The seismic reflection data were collected by a G3i digital seismometer made in Canada and two parallel 60 Hz longitudinal wave detector strings. The seismic source utilized a KZ-28 vibrator vehicle. The seismic dataset was acquired using a KZ-28 vibroseis vibrator at the center of each receiving station, with bilateral asymmetric reception. A vibrator spacing of 10 m and move-up distance of 2 m were utilized. The sweep frequency was 10–112 Hz, with a

length of 15 s. The record length was 1500 ms, with a 0.5 ms sample rate, and the receiving channels were 240.

The seismic reflection lines were conventionally processed by utilizing spectrum analysis, frequency filtering, speed sweep, and NMO correction (normal move-out) stacking to obtain a preliminary reflection seismic time image for quality monitoring during the collection of field data. Then, the seismic data were processed using predictive deconvolution, multiple velocity analysis, refractive static correction, residual static correction, migration, and noise suppression to highlight effective waves and suppress interference waves, thereafter forming the final reflection seismology time profile.

3.2. Trench Excavation

Aerial photos taken by a DJI Phantom 4 quadcopter were used to map lineaments that would potentially reveal the locations of active fault traces. We conducted unmanned aerial vehicle (UAV) surveys at a typical flying altitude of 100 m in Heli Town, a possible site of the YYF identified by seismic reflection data (Figure 2). We constructed dense point clouds, orthophotos, and high-resolution digital elevation models (DEM) from the photographs using the structure-from-motion method with Agisoft software (version 1.4.5). Based on our interpretation of the aerial photos and DEM, the YYF presented as a linear fault scarp across which we excavated a trench to reveal the fault traces of YYF. The depth of the trench was limited to 1.5 m. The walls of the trench were cleaned, photographed, and logged, and samples for radiocarbon and OSL dating were also collected from the trench to constrain the ages of faulted and unfaulted trench layers.

4. Results

4.1. Seismic Interpretation

4.1.1. Seismic Velocity Model

As a potential petroliferous basin, much of the seismic data were collected in the Sanjiang Basin [8,25–28], and we referred to these data to estimate the seismic velocity of different sedimentary sequences in this study (Table 1).

Table 1. Seismic velocity of different units in Tangyuan depression.

Strata		Lithology	P-Wave Velocity (m/s)
Covering layers	Quaternary	Sub-clay	1400
		Silty fine sand	1550
		Gravel	1800
	Neogene	Clay, mudstone, glutenite	1850
Bedrock	Paleogene	Mudstone, sandstone	2200
	Cretaceous	Andesite, rhyolite, tuff	>3000

To obtain the seismic velocity parameter used for the time depth conversion, the following methods were adopted: (1) A velocity spectrum was picked up every 50 CDP while analyzing the reflection data. (2) According to the strength distribution of the energy groups, the best superposition speed curve was selected, and then the superposition speed was calculated and converted to the average speed. (3) The time depth summary table of the whole area was obtained by comprehensively averaging the average velocities obtained from the shallow seismic data of each survey line (Table 2).

Table 2. The time depth summary table of this study.

Time (ms)	Depth (m)	Time (ms)	Depth (m)	Time (ms)	Depth (m)	Time (ms)	Depth (m)
10	7	270	249	530	558	790	930
30	23	290	271	550	584	810	962
50	38	310	293	570	611	830	994
70	54	330	316	590	638	850	1026
90	70	350	339	610	665	870	1058
110	87	370	362	630	693	890	1090
130	105	390	385	650	721	910	1122
150	124	410	409	670	750	930	1153
170	144	430	433	690	779	950	1183
190	164	450	457	710	809	970	1210
210	185	470	482	730	839	990	1238
230	206	490	507	750			
250	227	510	532	770			

4.1.2. Seismic Stratigraphy

The number of effective reflection wave groups that could be identified in the P-wave reflection profiles was different for each profile due to the influence of the geological structure and thickness of the overburden layers.

The regional geological map shows that the strata exposed in the study area were mainly composed of Neogene and Quaternary, of which the Quaternary were widely distributed and constituted the main covering layers in the area (Figure 2). Drilling revealed that the Quaternary strata consisted of Upper, Middle, and Lower Pleistocene, as well as Holocene strata. The thickness and composition of each stratum were relatively stable, and the interface was clear (Figure 3). Together with our seismic reflection data, we suggest 1–4 groups of effective reflection waves (T1, T2, T3, and Tg, Figure 4) for the seismic time profiles.

T1 developed between 50 and 70 ms, showing flattening in the whole area with relatively slight unevenness in some parts, and the reflection events could be traced continuously. T2 developed between 160 and 200 ms, which was relatively gentle across the whole area with slight fluctuations in some parts. The energy of T2 was strong, with obvious dual phases, and the reflection events had good continuity that could be tracked continuously. T3 developed between 260 and 300 ms, had strong energy and was biphasic locally. The reflection event had good continuity and could be tracked continuously. Tg developed between 410–450 ms and gradually deepened from the south to the north in the whole area, with strong amplitude. The event was biphasic and could be tracked continuously.

The collected borehole ZK1 was located 270 m south end of the profile L1, and the ZK2 was 100 m away from the southwest side of 1820CDP of L2-3 (Figure 2). The borehole data are displayed in Figure 3, in which the strata and geological attributes between each reflection group are given. According to the above seismic stratigraphic sequence calibration, we determined the corresponding relationship between the seismic sequence (T1, T2, T3, and Tg) and stratigraphic structure in the area, as shown in Table 3.

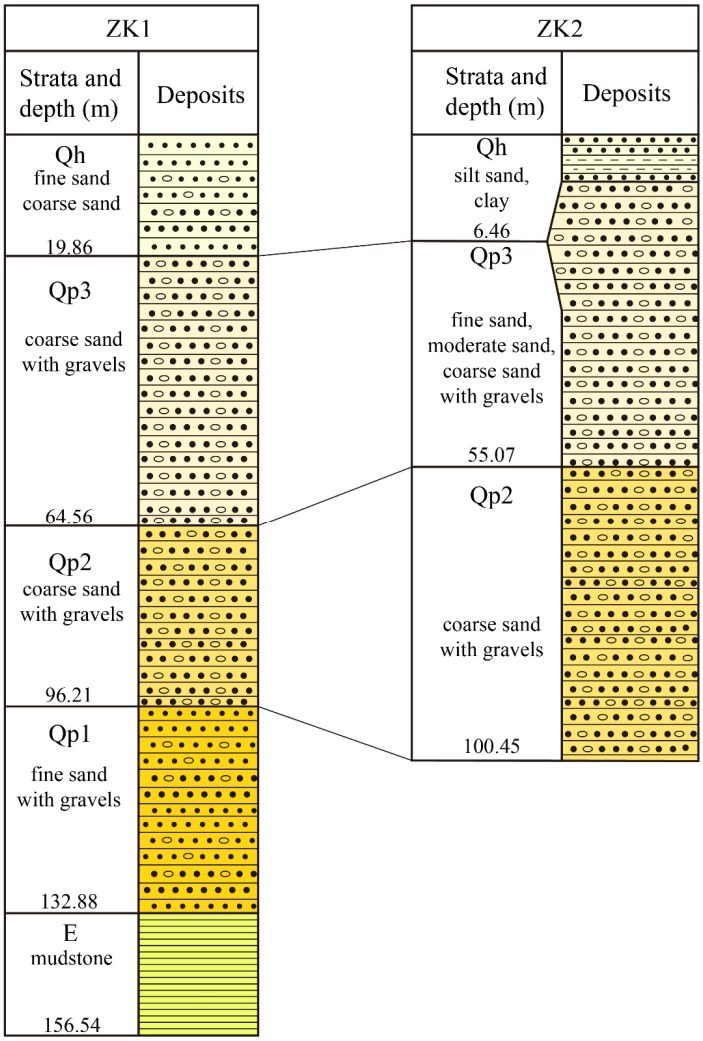

Figure 3. Drill column diagram of ZK1 and ZK2 with location indicated in Figure 2.

Table 3. The corresponding relationship between seismic sequences and stratigraphic structures.

	Strata	Seismic Reflection Groups	Lithology
Covering layers	Late Pleistocene to Holocene (Qp3-Qh)	T1	Middle-to-fine sand, middle-to-coarse sand, coarse sand with gravels, sub-clay
	Early-to-middle Pleistocene (Qp1-2)	T2	Middle-to-coarse sand, coarse sand with gravels, sand–gravel
	Pliocene (N2)	T3	Clay, silt
	Miocene (N1)	Tg	Sandstone, mudstone, conglomerate
Bedrock	Paleogene (E)		Sandstone, mudstone
	Cretaceous (K)		Andesite, tuff, rhyolite

4.1.3. Faults Revealed by Seismic Data

Four seismic profiles were created across the TFD (L1–L4, Figure 2), among which 10 fault planes were observed on L1, L2-2, L2-3, and L2-4, while no distinct abnormal reflection wave groups were observed on L2-1 or L3 (Figures 5 and 6).

(1) Faults on the L1

Three faulting points were observed on the L1: F1-1, F1-2, and F1-3. The F1-1 was located near 2960CDP of L1, where the seismic time profile showed that the reflection wave groups of bedrock were offset (Figure 7). At F1-1, the fault dipped in the NW direction, with a gentle angle of the Paleogene sandstone and an offset of about 10 ms (~9 m). The F1-1 was covered by early-to-middle Pleistocene (Qp1-2) sediments at the top, with a buried depth of about 125 ms (~110 m), which suggests that the F1-1 has not been active since the early-to-middle Pleistocene.

The F1-2 was located near 4120CDP of L1, causing intense deformation. It was offset at the top of Paleogene and early-to-middle Pleistocene reflectors, as well as at the bottom of the late Pleistocene to Holocene reflectors (Figure 7). Similarly to the adjacent F1-1, the F1-2 dipped in the NW direction, with a displacement of about 4 ms (~3 m) of the late Pleistocene sediments.

The F1-3 was located near 6310CDP of L1, resulting in the displacement of reflections in the Paleogene sediments (Figure 7). In contrast to the F1-1 and F1-2, the F1-3 presented as a normal fault with a steep angle dipping in the NW direction, which displaced the top of the Paleogene reflectors and those on the interior of the bedrock with offsets of 6 ms (~5 m) and 54 ms (~47 m), respectively. The top of F1-3, however, terminated in the early-to-middle Pleistocene, indicating that it is an inactive fault.

(2) Fault on L2-2

The F2-2 was located near 2420CDP of L2-2, as indicated by the break of reflections in the bedrock (Figure 8). The fault finished in the early-to-middle Pleistocene sediment, with a depth of ~120 ms (~104 m) into the ground, appearing as a steep and north-west-dipping normal fault with an offset of about 5 ms (~3 m) of bedrock (Figure 8). Different reflectors developed around 1500CDP south of the F2-2, the north of which is characterized by clear reflections, while to the south, no distinct reflections developed. Surface exposures suggest an angular, unconformable contact between the Paleogene to Neogene strata and Cretaceous volcanic rocks, and this bedrock, without obvious reflection wave groups, may be these volcanic rocks. We inferred that the different reflectors around the 1500CDP could be the unconformity between the Paleogene sandstones and mudstones and the Cretaceous volcanic sedimentary rocks which separated the Jiamusi Uplift from the Yilan-Yitong graben.

(3) Fault on L2B

The F2B was located near 1360CDP of L2B, reflected by the offset of Tg that may have been caused by the fault. Within L2B, the F2B appeared to be a normal fault, dipping NW with an offset of approximately 4 ms (3 m), as indicated by the height difference in the bedrock's surface (Figure 9). The top of F2B was covered by Quaternary deposits with a depth of about 120 ms (105 m), which suggests that the F2B has been inactive since the Quaternary.

At CDP900, south of the F2B, a group of gently dipping reflectors divided the Paleogene mudstone and sandstone from the Cretaceous volcanics, which was inferred to be the unconformity (Figure 9). North of the unconformity, the reflectors were well developed in the Paleogene, while no distinct reflectors were developed south of the unconformity in the Cretaceous.

(4) Fault on L2-3

The F2-3 was indicated by a break and drop of reflectors within the bedrock at around 4680CDP on the L2-3 profile, appearing as a steep, SE-dipping normal fault (Figure 10). Up

to the ground's surface, the F2-3 could be traced down to a depth of about 120 ms (103 m). Above the bedrock's surface (Tg), the reflections were continuous, which suggests that the F2-3 have been inactive since the Quaternary. North of the F2-3, the reflectors were in disarray and discontinuous; these could be the Cretaceous volcanic sedimentary rocks comprising the central uplift of the YYG. Those south of these were continuously well developed, and may be the Paleogene sandstone and mudstone constituting the eastern depression of the YYG.

(5) Faults on L2-4

Four faults were revealed by line L2-4 (F2-4-1, F2-4-2, F2-4-3, F2-4-4; Figure 11). The F2-4-1 was characterized by the displacement of reflectors in the bedrock at a depth of about 260 ms (245 m), presenting as a steep, NW-dipping normal fault (Figure 11). Upward, the reflections were continuous, without displacement in the Neogene or Quaternary, and the bedrock surface (Tg) was slightly twisted, suggesting that the F2-4-1 was active before the Neogene. North of the F2-4-1, the reflectors were well developed and clear; these could be Paleogene sandstone and mudstone as part of the western depression of the YYG. On the other hand, the reflectors were chaotic and unclear on the southern side and could be Cretaceous volcanic sediment belonging to the central uplift of the YYG.

The F2-4-2 was interpreted at around 6520CDP of L2-4, and was reflected by the discontinuity and offset of the reflectors in the bedrock (Figure 11). The fault dipped southeast with a gentle angle, presenting as a thrust fault. The top of F2-4-2 was limited in the bedrock, with a depth of about 170 m (200 ms), suggesting that this fault branch has been inactive since the Quaternary.

At around 10750CDP of L2-4, the underlying bedrock reflectors were deformed and displaced, showing a NW-dipping thrust of F2-4-3 with an offset of 6 ms (5 m) of the bedrock surface (Figure 11). The upper termination point of F2-4-3 was buried by the continuous reflections of T1 down to a depth of 140 ms (116 m), indicating that the fault was mainly active before the early-to-middle Quaternary. Similarly to the F2-4-3, the F2-4-4 was also characterized by the deformation and breakage of reflectors at 11250CDP of L2-4 (Figure 11). Contrastingly, the upper faulted point of F2-4-4 extended into the late Pleistocene sediments, demonstrating that the fault has been active since the late Pleistocene.

4.2. Paleoseismic Evidence

The YYF at Heli Town was visible in the late Quaternary sediment, as evidenced by fault scarps (Figure 12a). The vertical displacement of the geomorphic surface was determined by extracting elevation profiles perpendicular to the strike of the fault scarps from high-resolution DEM generated by UAV. The topographic profile showed that the fault scarp of the late Quaternary sediments was about 0.6 m in height. (Figure 12b,c). Trench excavation was conducted across the fault scarp in this study, which revealed seven distinct sedimentary units (Units 1–7) based on their composition, sedimentary facies, and structure (Figure 13). Unit 1 was composed of grayish-black sand and soil, and it constitutes the main plowlands in the northeastern China. Yellow earth and coarse sand with some gravel constituted unit 2. Samples from unit 2 showed ages of 5650 $\pm$ 30 y B.P. to 11.77 $\pm$ 0.51 ka (samples JMS-1 to JMS-3, as listed in Tables 4 and 5). Unit 3 was composed of blackish-gray soils that presented as lens-shaped, undulating layers. Small, light-gray gravels and sandy gravels made up Unit 4. Unit 5 was composed of cross-bedding alluvial gravels. Grayish-yellow, coarse gravels made up unit 6, which was interbedded with 10 cm of light-gray clay at the top between units 5 and 6. Unit 7 was composed of grayish-yellow alluvial gravels.

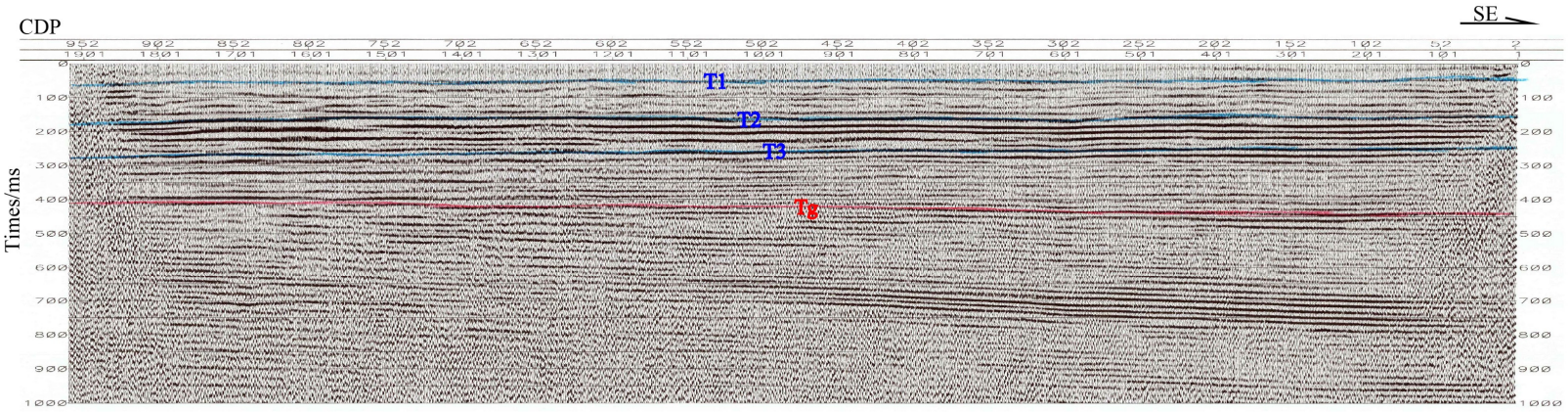

Figure 4. Seismic reflection profiles showing the four groups of reflection waves.

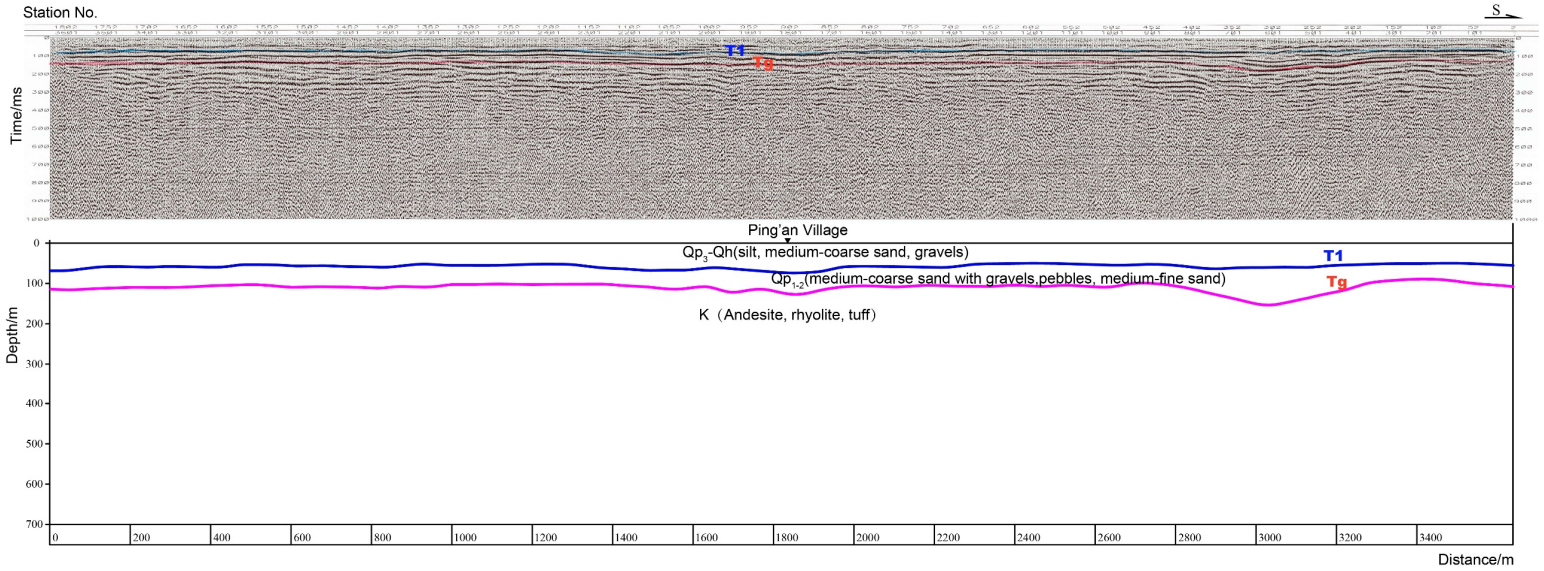

Figure 5. Seismic profiles of Line L2-1 and its interpretation.

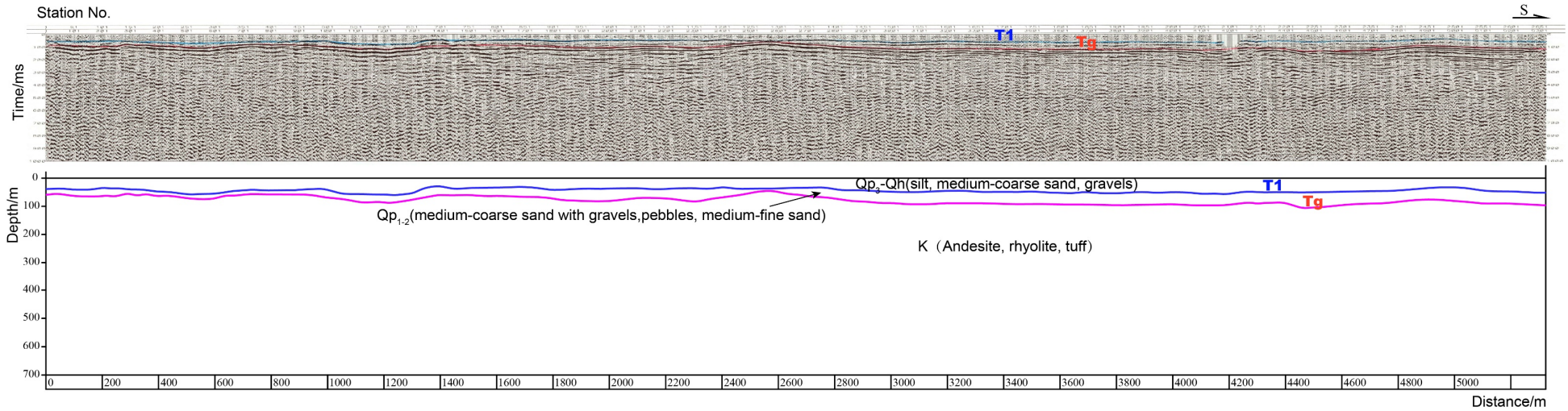

Figure 6. Seismic profiles of Line L3 and its interpretation.

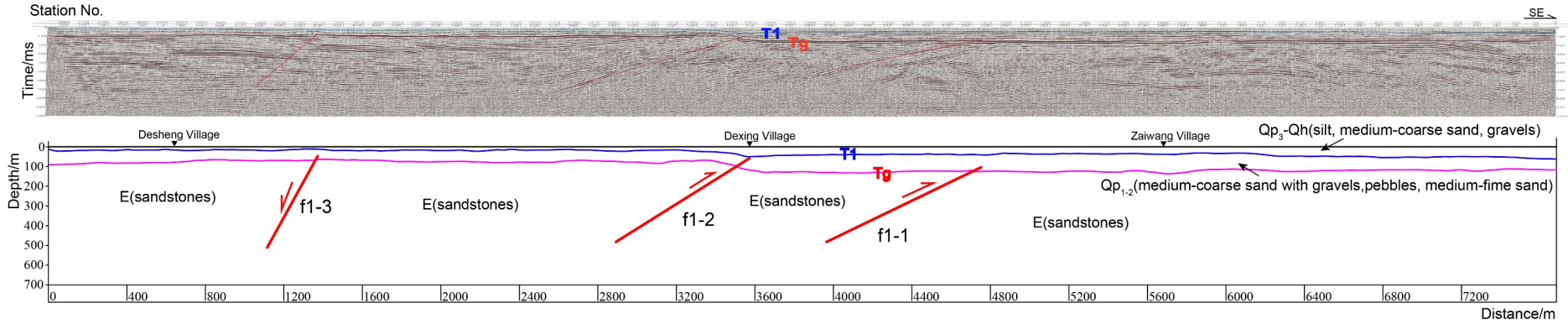

Figure 7. Seismic profiles of Line L1 and its interpretation.

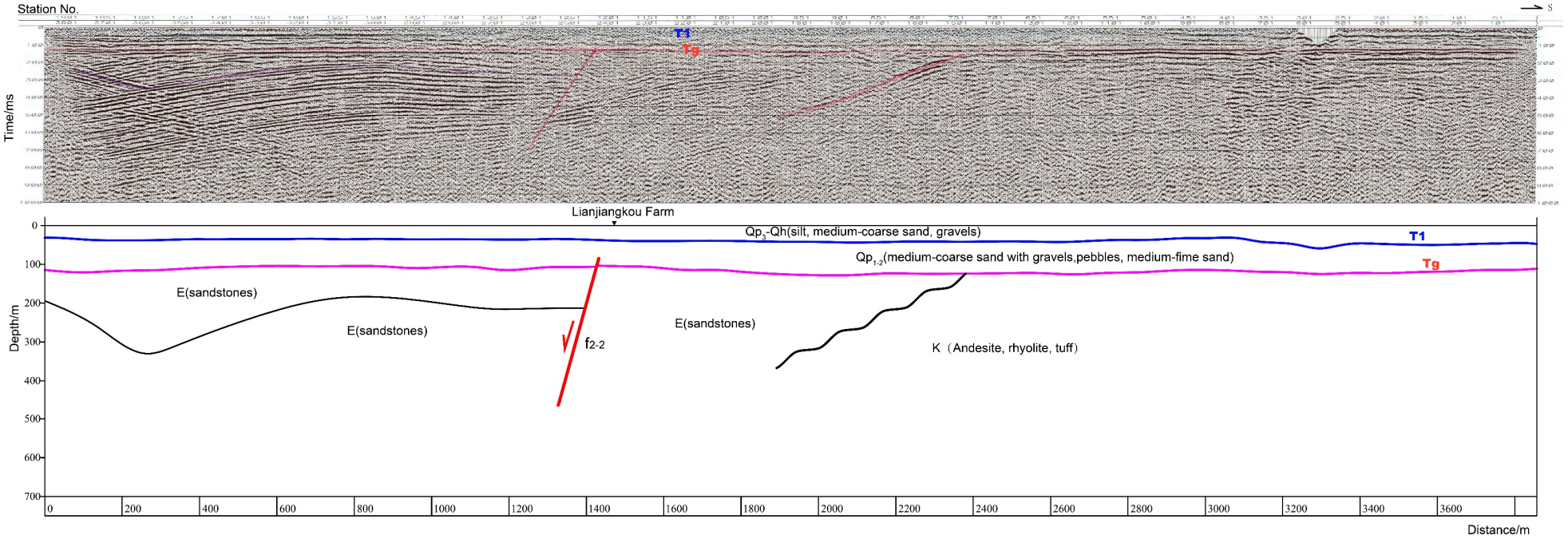

Figure 8. Seismic profiles of Line L2-2 and its interpretation.

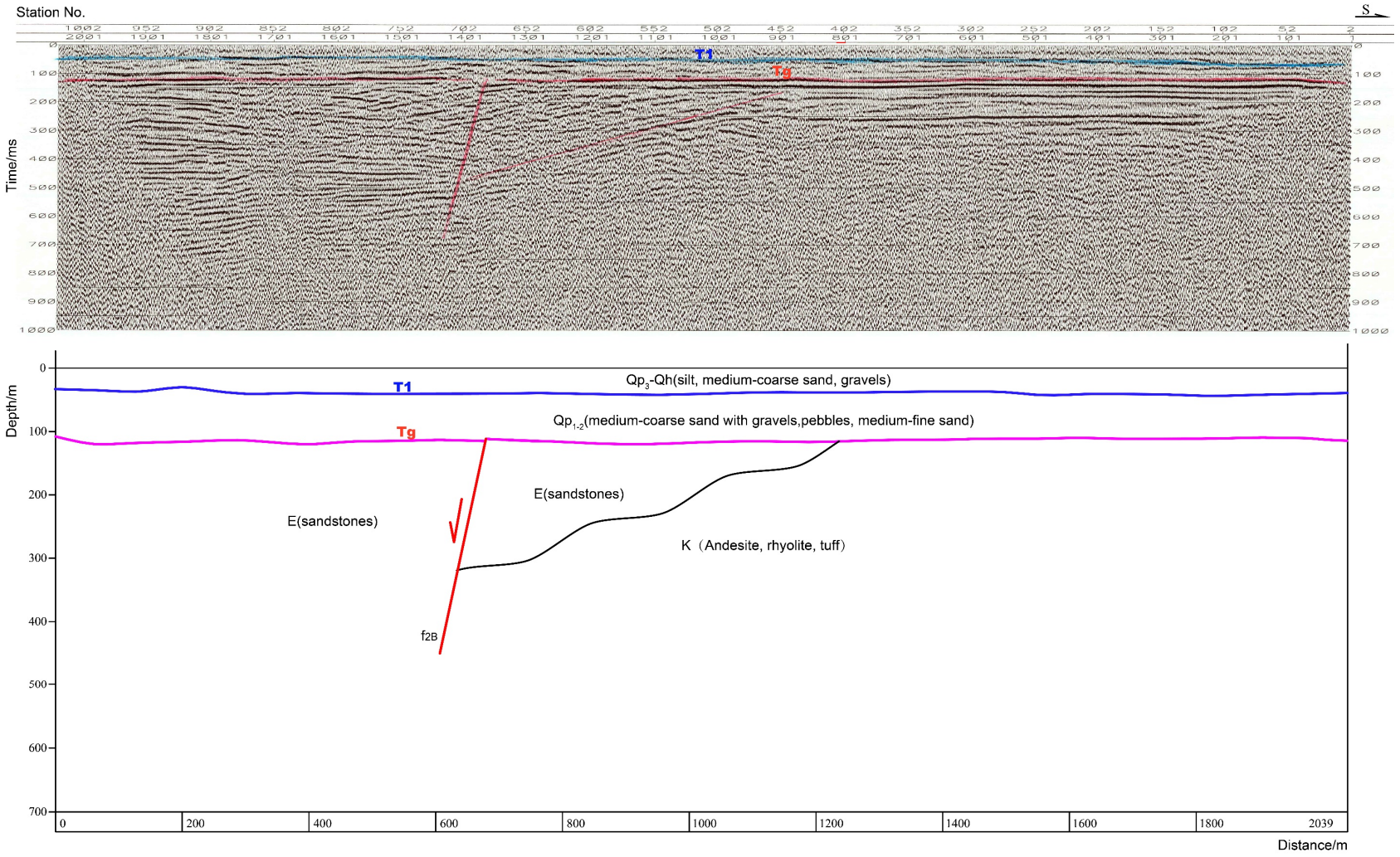

Figure 9. Seismic profiles of Line L2B and its interpretation.

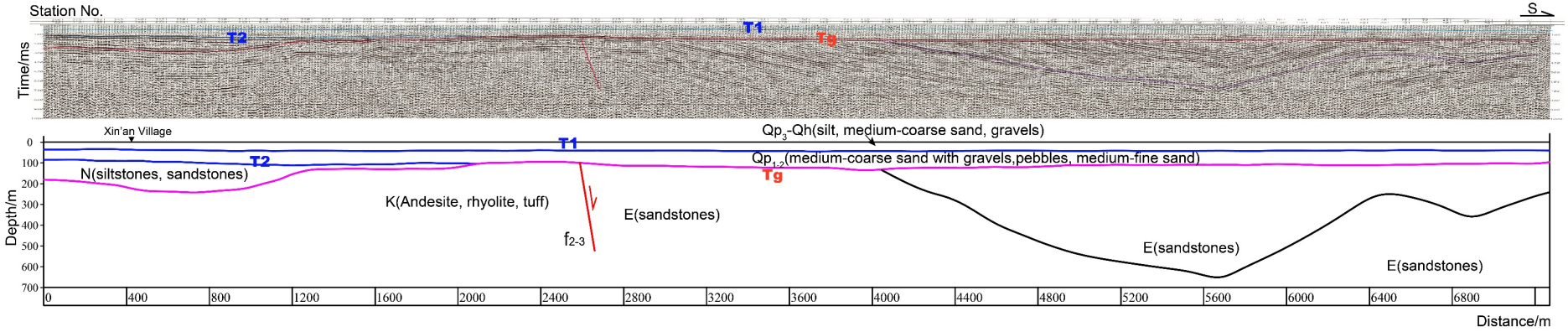

Figure 10. Seismic profiles of Line L2-3 and its interpretation.

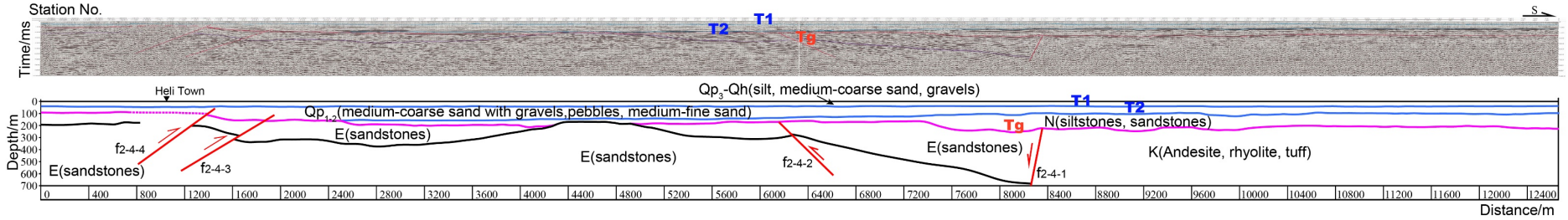

Figure 11. Seismic profiles of Line L2-4 and its interpretation.

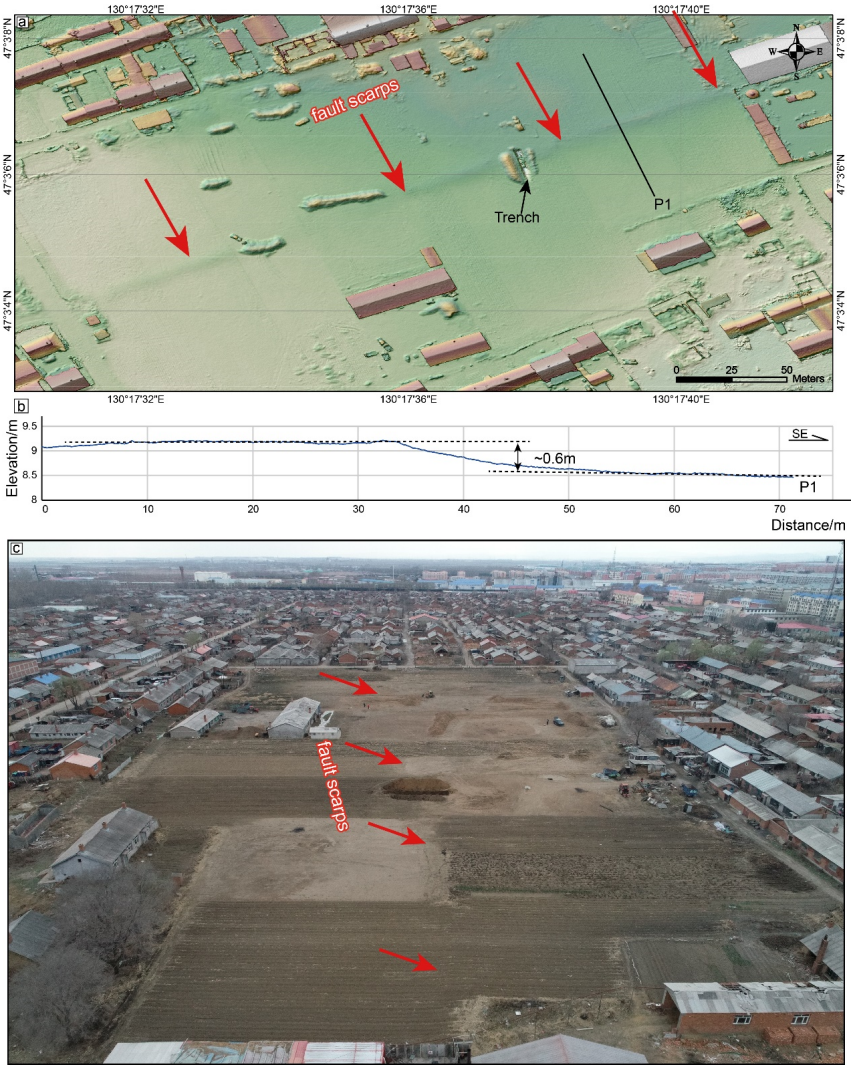

Figure 12. Site of the trench. (**a**) Fault scarps of the WYYF at Heli Town presented on the DEM derived from a UAV. (**b**) Topographic profile across the scarp with a height of about 0.6 m. (**c**) Photo of the fault scarp taken from a UAV.

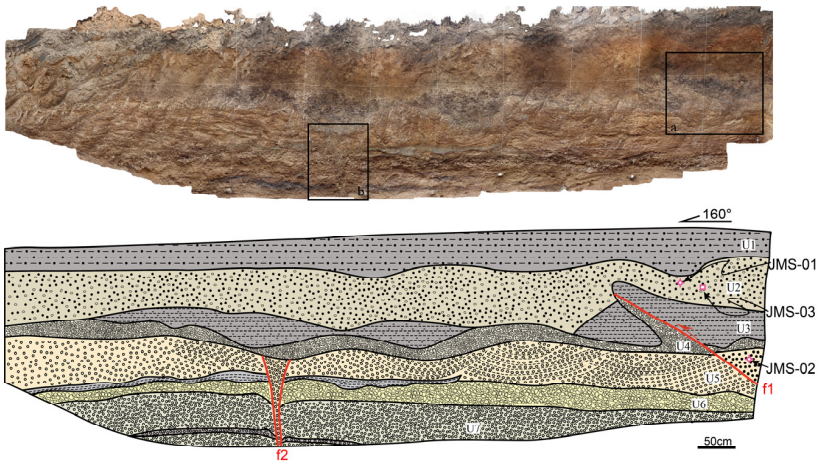

Figure 13. Trench photos and interpretation with the location of samples. The a and b show the detailed the fault features in Figure 14.

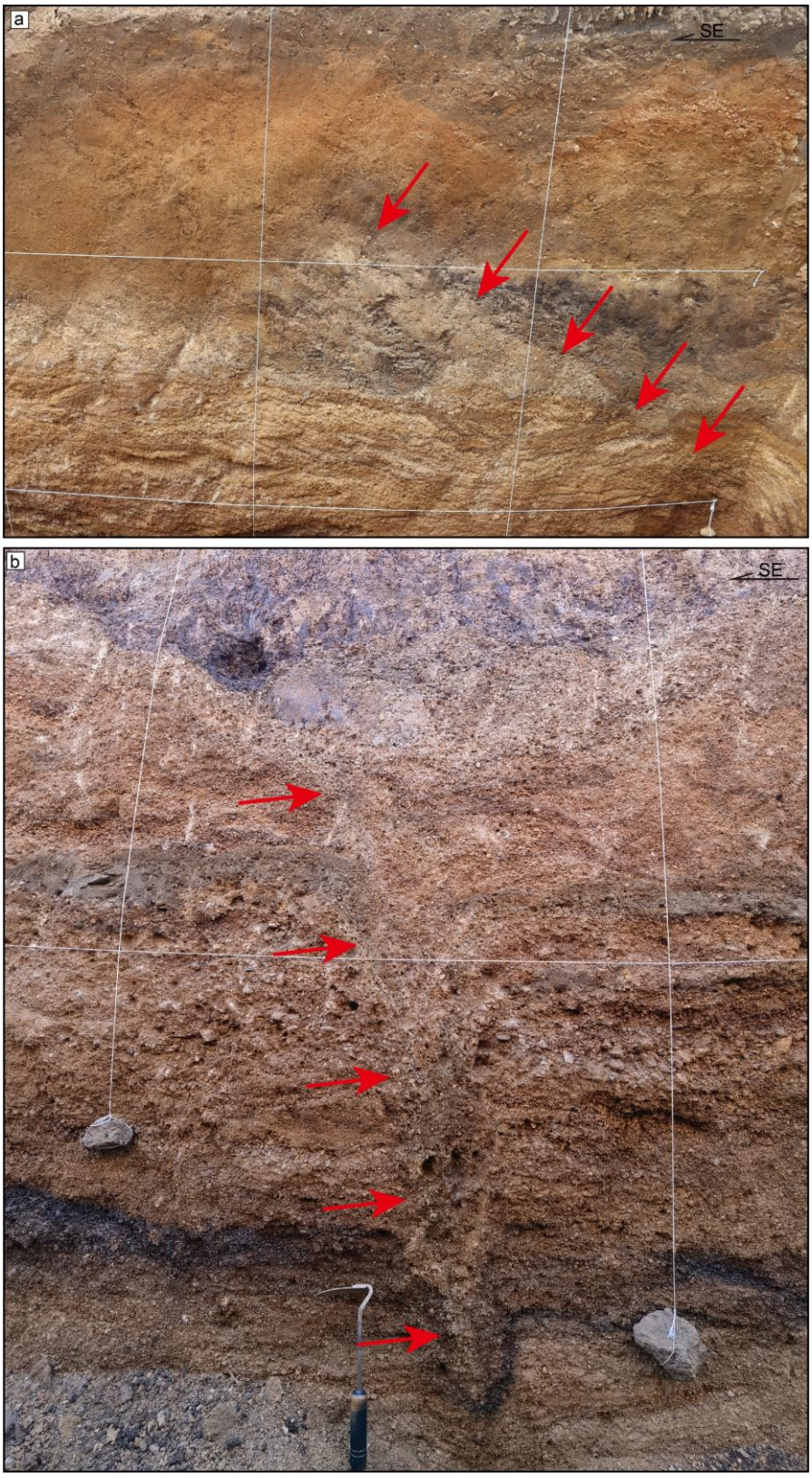

Figure 14. (**a**) Photograph of fault F1 revealed by the trench; (**b**) structure features of F2 indicated by oriented gravels.

Table 4. OSL dating results of samples from the trench.

Sample	Depth (m)	U (μg/g)	Th (μg/g)	K(%)	Water (%)	D (Gy/ka)	De (Gy)	Age (ka)
JMS-1	0.5	3.08 ± 0.1	13.8 ± 0.28	2.69 ± 0.02	15.12	3.92 ± 0.15	46.16 ± 1.04	11.77 ± 0.51
JMS-2	2	1.18 ± 0.01	5.37 ± 0.24	4.16 ± 0.03	5.00	4.85 ± 0.22	119.57 ± 7.12	24.64 ± 1.85

Table 5. Radiocarbon results of the sample from the trench.

Sample	Beta ID *	Conventional Age † (yr B.P.)	Calibrated Age ‡ (Cal B.P.)	Calibrated Calendar Age (B.C.)	Description
JMS-3	613471	5650 ± 30	6495-6390	4546-4441	Organic soil

* Samples were analyzed at Beta Analytic Inc., Miami, FL, USA. † Radiocarbon ages were measured using accelerator mass spectrometry (AMS) and are referenced to the year A.D. 1950. The analytical uncertainties are reported at 2σ. ‡ Dendrochronologically calibrated calendar age by OxCal 4.3 [29,30].

The trench wall also revealed the presence of two fault branches (F1–F2) (Figure 13). Fault F1 was characterized by the deformation of U3 and U4 (Figure 14). Fault F2 presented distinct fissures and bending gravels within U5, U6, and U7, causing the displacement of the gray clay interbedded in U6 (Figure 14).

5. Discussion

5.1. Geometry and Kinematics of the Northmost Yilan-Yitong Fault

Based on the shallow seismic profiles, four fault branches (F1-1, F9, F1-3 and F1-2, Figure 2) were identified at the northmost point of the YYF, described as follows:

The F1-2 and F2-4-4 are both northwest-dipping reverse faults with similar strikes in their spatial distributions, which could be connected to F1 fault, as is consistent with the western branch of the YYF. The NE-trending reverse F1 fault was steep at the top and gentle at the bottom, as shown by the shallow seismic reflection data. According to the seismic sequence, the F1 fault has been active since the late Pleistocene.

The northwest-dipping reverse faults F1-1 and F2-4-3 could be linked to fault F9, with a burial depth of about 110-116 m, which suggests that the F9 has been inactive since the early Pleistocene. Based on the geometry revealed by the seismic data, we inferred that the F1 and F9 would be the two main branches of the WYYF, and that they would connect into one fault at a certain depth.

The northwest-dipping normal fault F1-3 faulted in the early-to-middle Pleistocene strata, which indicates that F1-3 has been inactive since the early-to-middle Pleistocene. Fault F1-2, the eastern branch of YYF, comprised the steep, northwest-dipping normal fault F2-2-1 as well as F2B-1, with a burial depth of about 105 m. This suggests that the F1-2 has been an inactive fault since the early Pleistocene.

We identified two fault branches (F1 and F2) on the trench wall based on the displacement of sedimentary units and structural deformation. The F1 cut unit 3, but did not displace the bottom of unit 2, while the F2 was covered by unit 4, which suggests that F1 occurred after F2. We estimated that the most recent paleoearthquake event occurred before the deposition of unit 2 and after that of unit 3. We obtained two possible ages for unit 2 by OSL and 14C dating, with ages of about 11 ka and 4.5 ka, respectively (Tables 4 and 5). Based on the regional Quaternary strata distribution, we suggest that the 4.5 ka estimate may be close to the real age of unit 2. The depth of samples JMS-01 and JMS-03 was about 0.5 m, corresponding to the Holocene. The dating results suggest that the most recent paleoearthquake occurred before 4.5 ka, which is different from other segments of YYF [11]. Previous studies have suggested that the earthquake recurrence interval could be several to tens of thousands of years [15]. Compared with the earthquake recurrence interval, the Tangyuan segment of YYF faces a relatively low seismic risk. However, the seismic hazard assessment requires more evidence, and more research is needed in the future.

5.2. Cenozoic Evolution of Yilan-Yitong Graben

The seismic time section revealed significantly different reflect signals within the bedrock at around 1500CDP of L2-2 and 900CDP of L2B, south of which no obvious reflectors developed, while dense reflectors developed to the north within the bedrock. The different reflectors were bounded by a nonconforming surface, which appears as a group of gently dipping reflections in the seismic time section. The unconformity strikes NEE and divides the Jiamusi uplift from the Yilan-Yitong graben, the west of which is dominated by Paleogene sandstone and mudstone in the Yilan-Yitong graben, and the east of which is occupied by the Cretaceous volcanic sedimentary rocks of the Jiamusi uplift.

Three NE-trending structures exist from the northwest to southeast in the Yilan-Yitong graben: the western depression, central rise, and eastern depression (Figure 15). Based on the seismic profiles, the eastern depression is 6.3 km wide, the central rise is 6.7 km wide, and the width of the western depression exceeds 8.3 km. The western and eastern depressions are composed of Paleogene strata, and the central rise is dominated by the Cretaceous. Additionally, the sand and mudstone sequence in the eastern and western depressions appeared as gentle folds, as revealed by the reflectors in the bedrock. The western depression is composed of two anticlines and two synclines distributed alternately on the seismic data (Figure 15), while the eastern depression is composed of two anticlines sandwiched by a syncline (Figure 15). Only the southern-most anticline shows a local bend located at the 350CDP of L2-3 and the 2650CDP of L2-2, which represents the overlapping parts of the two survey lines, that is, they are conformal bends on the same anticline. The deformed Paleogene and overlying Neogene strata suggest that the folds in the Yilan-Yitong graben were formed after the end of the Paleogene.

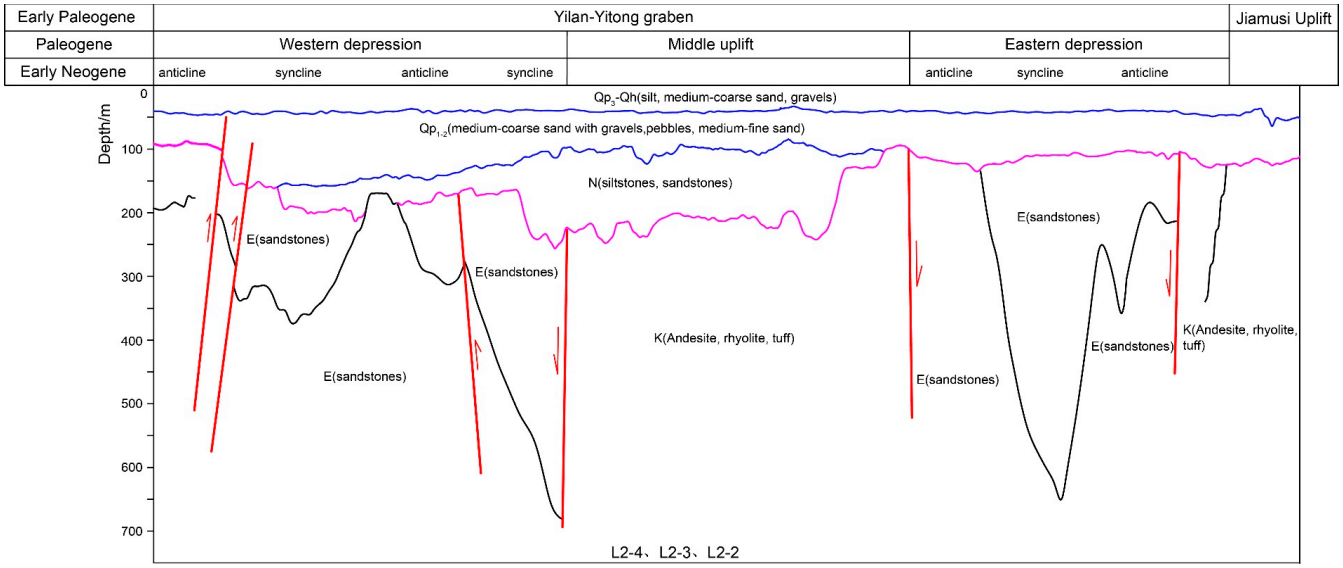

Figure 15. Tectonic framework across the TFD revealed by the seismic reflection data.

The seismic time sections suggest that the Neogene strata were distributed locally, thinly in the west and thickly in the east, which is consistent with the drilling data. However, the spatial distribution difference in the thickness of the Neogene strata indicate that the Yilan-Yitong graben formed huge thick deposits in the Paleogene, and then the Neogene appeared to have different spatial subsidence and rise characteristics. To the west, the graben, i.e., the rising section, resulted in sporadic deposition of Neogene strata, while the Neogene deposits were widespread, and the thickness increased significantly to the east. Only in the early Pleistocene did the whole graben and its surrounding area have a large range of subsidence.

6. Conclusions

(1) North of Tangyuan County, the YYF is composed of two main branches, of which the western YYF branch is a late-Pleistocene active fault and the eastern one is a middle-to-early-Pleistocene fault.

(2) Field investigation and trench excavation suggested that the most recent paleoearthquake may have occurred before about 4.5 ka along the Tangyuan segment of the YYF. Compared with the seismic recurrence interval, the risk of a large earthquake in Tangyuan is relatively low, but this requires more evidence in order to be verified.

(3) The seismic reflection data and sedimentary sequence reveal that the YYF north of Tangyuan is composed of three tectonic belts: a western depression, a central bulge, and an eastern depression. Each tectonic belt is composed of several small folds formed from the end of Paleogene to the beginning of Neogene. After the Neogene, differing subsidence and uplift arose in various parts of the YYF, and after the early Pleistocene, it showed consistent subsidence.

In this paper, we provided the shallow geometry of the Tangyuan segment of the YYF and preliminarily estimated the times of paleoearthquake occurrence. In the future, we suggest that focus be placed on deep structural and detailed paleoearthquake sequences to discuss tectonic origins and seismic hazard risks.

Author Contributions: Conceptualization, Q.W. and G.H.; methodology, W.M.; formal analysis, W.M. and G.H.; investigation, Q.W., G.H. and M.Z.; writing—original draft preparation, Q.W.; writing—review and editing, Q.W. and G.H.; visualization, G.H. and M.Z.; funding acquisition, W.M. All authors have read and agreed to the published version of the manuscript.

Funding: This research was funded by the National Key Research and Development Project of China, grant number 2022YFC3003501.

Institutional Review Board Statement: Not applicable.

Informed Consent Statement: Not applicable.

Data Availability Statement: No new data were created or analyzed in this study.

Conflicts of Interest: The authors declare no conflicts of interest.

References

1. Bai, Z.; Zhang, Z.; Wang, Y. Crustal structure across the Dabie–Sulu orogenic belt revealed by seismic velocity profiles. *J. Geophys. Eng.* **2007**, *4*, 436–442. [CrossRef]
2. Deng, Y.; Fan, W.; Zhang, Z.; Badal, J. Geophysical evidence on segmentation of the Tancheng-Lujiang fault and its implications on the lithosphere evolution in East China. *J. Asian Earth Sci.* **2013**, *78*, 263–276. [CrossRef]
3. Lin, A.; Miyata, T.; Wan, T. Tectonic characteristics of the central segment of the Tancheng–Lujiang fault zone, Shandong Peninsula, eastern China. *Tectonophysics* **1998**, *293*, 85–104. [CrossRef]
4. Wang, W.; Jin, Q.; Ma, Z. Meso-Cenozoic Evolution of the Tanlu Fault and Formation of Sedimentary Basins. *Acta Geol. Sin.-Engl. Ed.* **1998**, *72*, 350–362.
5. Yuan, X. On continental basal structure in China. *Chin. J. Geophys.* **1995**, *38*, 448–459. (In Chinese with English Abstract)
6. Chang, E.Z. Collisional orogene between north and south China and its eastern extension in the Korean Peninsula. *J. Southeast Asian Earth Sci.* **1996**, *13*, 267–277. [CrossRef]
7. Gu, C.; Zhu, G.; Zhai, M.; Lin, S.; Song, L.; Liu, B. Features and origin time of Mesozoic strike-slip structures in the Yilan-Yitong Fault Zone. *Sci. China Earth Sci.* **2016**, *59*, 2389–2410. [CrossRef]
8. Kamali, Z.; Nazari, H.; Rashidi, A.; Heyhat, M.R.; Khatib, M.M.; Derakhshani, R. Seismotectonics, Geomorphology and Paleoseismology of the Doroud Fault, a Source of Seismic Hazard in Zagros. *Appl. Sci.* **2023**, *13*, 3747. [CrossRef]
9. Kang, D.; Shen, W.; Ning, J.; Ritzwoller, M.H. Seismic evidence for lithospheric modification associated with intracontinental volcanism in Northeastern China. *Geophys. J. Int.* **2016**, *204*, 215–235. [CrossRef]
10. Min, W.; Liu, Y.; Jiao, D.; Shen, J.; Pan, X. Evidence for Holocene activity of the Yilan-Yitong fault, northeastern section of the Tan-Lu fault zone in Northeast China. *J. Asian Earth Sci.* **2013**, *67–68*, 207–216. [CrossRef]
11. Tian, Z.; Du, Y. Formation and evolution of the Yilan-Yitong graben. *Tectonophysics* **1987**, *133*, 165–173. [CrossRef]
12. Wang, E.; Meng, Q.; Burchfiel, B.C.; Zhang, G. Mesozoic large-scale lateral extrusion, rotation, and uplift of the Tongbai–Dabie Shan belt in east China. *Geology* **2003**, *31*, 307–310. [CrossRef]

13. Xu, M.; Li, Y.; Hou, H.; Wang, C.; Gao, R.; Wang, H.; Han, Z.; Zhou, A. Structural characteristics of the Yilan–Yitong and Dunhua–Mishan faults as northern extensions of the Tancheng–Lujiang Fault Zone: New deep seismic reflection results. *Tectonophysics* **2017**, *706–707*, 35–45. [CrossRef]
14. Yu, Z.; Yin, N.; Shu, P.; Li, J.; Wei, Q.; Min, W.; Zhang, P. Late Quaternary paleoseismicity and seismic potential of the Yilan-Yitong Fault Zone in NE China. *J. Asian Earth Sci.* **2018**, *151*, 197–225. [CrossRef]
15. Zhao, T.; Zhu, G.; Lin, S.; Wang, H. Indentation-induced tearing of a subducting continent: Evidence from the Tan–Lu Fault Zone, East China. *Earth-Sci. Rev.* **2016**, *152*, 14–36. [CrossRef]
16. Zhu, G.; Liu, G.S.; Niu, M.L.; Xie, C.L.; Wang, Y.S.; Xiang, B. Syn-collisional transform faulting of the Tan-Lu fault zone, East China. *Int. J. Earth Sci.* **2009**, *98*, 135–155. [CrossRef]
17. Zhang, L.; Barnden, J.A.; Hendley, R.J.; Lee, M.G.; Wallington, A.; Wen, Z. Affect detection and metaphor in e-drama. *Int. J. Contin. Eng. Educ. Life Long Learn.* **2008**, *18*, 234–252. [CrossRef]
18. Deng, Q.; Ran, Y.; Yang, X.; Min, W.; Chu, Q. *Active Tectonics Map of China*; Seismology: Beijing, Chian, 2007. (In Chinese)
19. Gu, C.; Zhu, G.; Zhang, S.; Liu, C.; Li, Y.; Lin, S.; Wang, W. Cenozoic evolution of the Yilan–Yitong Graben in NE China: An example of graben formation controlled by pre-existing structures. *J. Asian Earth Sci.* **2017**, *146*, 168–184. [CrossRef]
20. Li, Z.; Jia, D.; Chen, W.; Zhang, Y.; Wang, M.; Li, Y.; Li, H.; Li, S.; Zhou, X.; Wu, L.; et al. Structural deformation and evolution of right-lateral strike-slip tectonics of the Liaohe western depression during the early Cenozoic. *J. Asian Earth Sci.* **2013**, *77*, 1–11. [CrossRef]
21. Tang, D.-Q.; He, S.; Chen, H.-H. Fault system's characteristics of Yitong Basin and its evolution. *J. Jilin Univ. Earth Sci. Ed.* **2009**, *39*, 386–395.
22. Tang, D.; Chen, H.; Sun, J.; Zhang, H.; Chen, L. Cenozoic tectonic evolution of the Yitong part of the Tan-lu fault zone and its control on Yitong basin. *Geotecton. Metallog.* **2010**, *34*, 340–348.
23. Shen, Y.; Liu, C.; Jiang, L.; Wang, S.; Wang, D. Fault characteristics and analysis of tectonic styles in Tangyuan Fault-depression. *J. Jilin Univ. (Earth Sci. Ed.)* **2006**, *36*, 104–108.
24. Yang, J.-G.; Liu, J.-L.; Wu, H.-Y.; Liu, C.-G. The characteristics and evolvement of the tectonic in Tangyuan rift in northern Heilongjiang. *J. Daqing Pet. Inst.* **2007**, *31*, 19.
25. Guo, S.-B.; Wang, H. Sequence stratigraphic characteristics and hydrocarbon prospect of Mesozoic Formation in Suibin Depression, Sanjiang Basin. *Pet. Explor. Dev.* **2008**, *35*, 44–51. [CrossRef]
26. Wang, D.; Jia, L. Study on Seismic Geological Conditions and Acquisition Techniques in Sanjiang Basin. *Geophys. Prospect. Pet.* **2006**, *45*, 423–426. (In Chinese)
27. Wu, W.; Huang, J.; Li, X.; Liu, Z.; Zhu, H. Crustal structure in the Dasanjiang basin and its adjacent areas. *Acta Seismol. Sin.* **2022**, *44*, 286–301. [CrossRef]
28. Zhang, F.-Q.; Chen, H.-L.; Yang, S.-F.; Feng, Z.-Q.; Wu, H.-Y.; Batt, G.E.; Zhao, X.-Q.; Sun, M.-D.; A, M.-N.; Wang, S.-H.; et al. Late Mesozoic–Cenozoic evolution of the Sanjiang Basin in NE China and its tectonic implications for the West Pacific continental margin. *J. Asian Earth Sci.* **2012**, *49*, 287–299. [CrossRef]
29. Ramsey, C.B. Bayesian analysis of radiocarbon dates. *Radiocarbon* **2009**, *51*, 337–360. [CrossRef]
30. Reimer, P.J.; Bard, E.; Bayliss, A.; Beck, J.W.; Blackwell, P.G.; Ramsey, C.B.; Buck, C.E.; Cheng, H.; Edwards, R.L.; Friedrich, M.; et al. IntCal13 and Marine13 radiocarbon age calibration curves 0–50,000 years cal BP. *Radiocarbon* **2013**, *55*, 1869–1887. [CrossRef]

Disclaimer/Publisher's Note: The statements, opinions and data contained in all publications are solely those of the individual author(s) and contributor(s) and not of MDPI and/or the editor(s). MDPI and/or the editor(s) disclaim responsibility for any injury to people or property resulting from any ideas, methods, instructions or products referred to in the content.